Journal of Building Engineering 66 (2023) 105877

Contents lists available at ScienceDirect

Journal of Building Engineering

journal homepage: www.elsevier.com/locate/jobe

Comparative study of alternative equivalent frame approaches for the seismic assessment of masonry buildings in OpenSees

M.V. Requena-Garcia-Cruz [a,*], S. Cattari [b], R. Bento [c], A. Morales-Esteban [a]

[a] Department of Building Structures and Geotechnical Engineering, University of Seville, Av. Reina Mercedes, 2, 41012, Seville, Spain
[b] Department of Civil, Chemical and Environmental Engineering (DICCA), University of Genoa, Via Montallegro 1, 16145, Genoa, Italy
[c] Instituto Superior Técnico, Universidade de Lisboa, Av. Rovisco Pais, 1049-001, Lisbon, Portugal

ARTICLE INFO

Keywords:
Masonry structures
Equivalent frame models
OpenSees
Nonlinear analyses

ABSTRACT

The equivalent frame (EF) idealisation of masonry structures is widely used in engineering structures. Despite its simplifications, reliable numerical models can be produced to calculate the seismic behaviour of unreinforced masonry (URM) buildings. Different EF modelling approaches have been implemented in commercial software specifically conceived for performing nonlinear analyses on URM buildings (such as 3Muri, adopted in this study). Furthermore, the adoption of such an approach is also possible in general-purpose structural analyses software packages, such as OpenSees, through an ad hoc implementation of analysts. The aim of this paper is to compare various EF modelling approaches by adopting alternative nonlinear beam-elements in OpenSees belonging to the distributed and the lumped plasticity. To this aim, the responses of some benchmark cases study available in the literature from the "URM nonlinear modelling-benchmark project" within the context of ReLUIS projects have been adopted to preliminary test the reliability of the alternative approaches considered. In particular, they consist of some single panels and a trilith, for which the results of various software are already available. In the paper, the results obtained with OpenSees have been more in-depth compared with 3Muri, which is assumed as representative of a larger set of EF models adopted in engineering-practice (having already verified in previous works that it provides a reasonable scatter with other software package options). Then, the analyses have been extended as well to a 3D building representative of the neighbourhood of 'El Plantinar' in Seville. An accurate comparison has been carried out in terms of generalised forces, drifts and damage at an element and at a global scale. The results have shown that the method proposed in this manuscript allows using OpenSees to calculate masonry structures with the EF approach with a good agreement to other engineering-practice oriented tools. Thus, this outcome may constitute, in future research, the basis for exploiting the potential and versatility of OpenSees in accounting for other tricky phenomena: the soil-foundation-structure interaction.

* Corresponding author.
E-mail addresses: mrequena1@us.es (M.V. Requena-Garcia-Cruz), serena.cattari@unige.it (S. Cattari), rita.bento@tecnico.ulisboa.pt (R. Bento), ame@us.es (A. Morales-Esteban).

https://doi.org/10.1016/j.jobe.2023.105877
Received 26 July 2022; Received in revised form 9 December 2022; Accepted 9 January 2023
Available online 10 January 2023

List of symbols and abbreviations

Geometrical parameters

h	panel height
l	panel width
t	panel thickness
β	correction coefficient depending on aspect ratio/slenderness
h_0	contraflexure point height
h_{eff}	effective height of the pier (length of the deformable portion)
l_{eff}	effective length of the spandrel *Constitutive laws*
σ_0	mean normal stress on the panel (computed referring to the gross area of the transversal section), $\sigma_0 = N/lt$
N	axial load at the centre of the panel
V	shear force
M_{u}	ultimate bending moment
V_{u}^{PF}	corresponding ultimate shear associated with the flexural mode
V_{t}	diagonal cracking shear response (Turnšek and Čačovič criterion)
f_{cu}	masonry compressive crushing strength
ϵ_{cp}	strain at peak compressive stress
ϵ_{cu}	strain at compressive crushing stress
ϵ_{tp}	strain at peak tensile strength
E	Young's modulus
E_0	initial stiffness for the masonry nonlinear behaviour
G	shear modulus

Other parameters

W	specific weight A_{s} area of the steel rebar in the reinforced concrete ring beam
f_{y}	mean yield strength of steel. Subindex 'k' refers to characteristic value

Masonry properties

CF	confidence factor (applied only to the strength parameters). The 'design' values are obtained by applying the confidence factor CF to the mean values of the assigned strength. Subindex 'd' refers to design value
f_{c}	compressive strength in vertical direction. Subindex 'k', 'm' and 'rc' refer to characteristic value, masonry and reinforced concrete, respectively
τ_0	diagonal cracking shear strength of masonry panels
f_{h}	masonry compressive strength in horizontal direction
f_{b}	brick compressive strength
f_{m}	mortar compressive strength
f_{t}	masonry tensile strength
K_{e}	initial stiffness of panels
c	cohesion of the masonry wall
μ	friction angle of the masonry wall

Miscellaneous

EF	Equivalent frame
OS	OpenSees
3 M	3Muri
NLS	Nonlinear static
ZL	Zero Length element
DP	Distributed plasticity
LP	Lumped plasticity
DI	Displacement
DF	Deformation
E	Empirical
A	Analytical

1. Introduction

There are several modelling strategies to study the global response of unreinforced masonry (URM) structures, such as the finite element (FE) models, based on the continuum constitutive laws models (CCLM), and the equivalent frame (EF) method [1,2]. The FE

models are complex to apply to a large amount of nonlinear analyses due to their high computational cost and to the large number of input data required [3]. This modelling approach is usually used for irregular, complex or strategic structures. Contrariwise, the EF idealisation of masonry structures is widely used in engineering practice due to its computational efficiency and the reduced quantity of input data [4]. Nevertheless, it is subjected to certain simplifications. The EF approach is based on the assumption that the nonlinear response of each masonry wall may be concentrated in specific panels (*piers* – vertical panels; and *spandrels* – horizontal panels that connect piers). The remaining parts of the walls are usually idealised as rigid nodes, since in most cases no seismic damage was observed in them, as discussed in Refs. [5–9]. Both the piers and the spandrels are usually conceived as nonlinear beam models able to account for the main failure modes of the walls (bending and shear) [10]. The EF approach is particularly suitable in the case of structures dominated by a box-like behaviour, i.e. characterized by the activation of the in-plane response of URM walls. This paper focuses only to this type of response. The EF approach is also explicitly suggested in various seismic codes for the assessment of URM structures [11–13] and it easily allows introducing other structural elements such as tie elements (the behaviour of URM buildings is affected by horizontal diaphragms/elements) or even RC beams or columns to assess mixed structures [5].

Despite its simplifications, the EF idealisation of URM walls can produce reliable results, as it has been concluded in several works [14–17]. In Ref. [18], comparisons between the results obtained with FE macro and micro models and other EF schemes were performed. Similarly, in Refs. [19,20], a quite accurate comparison between CCLM models and EF models has been performed by considering both regular and irregular opening layout. In Refs. [4,21], nonlinear static (NLS) analyses were carried out considering different software packages based on the EF approach. These works obtained rather limited variations on the initial lateral stiffness, the base-shear, the displacement capacity, and the damage of examined 3D structures when the modelling is made with consistent assumptions varying the software package adopted. Nevertheless, it was pointed out that a careful selection of appropriate criteria is needed when performing analyses of URM systems to obtain reliable results [22].

The overall behaviour of URM structures mainly depends on the adoption of a suitable strength and drift/deformation domains of single elements/panels to account for each failure mode [23]. During the nonlinear static analysis, the axial load acting in panels changes due to the redistribution of forces produced by the application of horizontal load patterns. Therefore, the value of the strength of the panels also varies during the analysis. How much the capability of EF models of considering such issue affects the results is investigated in the paper. Moreover, as pointed out in Ref. [24], the axial load ratio, the shear span and the wall size are among the factors that most influence the drift capacity, which is one of parameters mostly affecting the ultimate displacement capacity of pushover curves deriving from NLS analyses.

Different EF modelling approaches have been implemented in commercial software which are specifically conceived for performing nonlinear analyses on URM buildings. Recently, in the "*URM nonlinear modelling* – Benchmark project" carried out within the ReLUIS projects (*Rete dei Laboratori Universitari di Ingegneria Sismica - Italian Network of University Seismic Laboratories*) [25], the proper use of software packages employed by professionals and researchers for the nonlinear modelling and the seismic assessment of URM buildings has been investigated by outlining a set of benchmark structures. Within this project, various software packages, based on different modelling approaches – including the EF one –, have been used and compared.

Instead of using commercial software, EF modelling approaches can be also developed in general-purpose structural analyses software packages. However, the tricky issues consequent to their implementation as well as the advantages and the limitations have not yet been accurately analysed. Given this, the aim of this paper is to compare different EF modelling approaches by adopting alternative nonlinear beam-elements in OpenSees, belonging to the distributed and the lumped plasticity. The more specific scopes of the paper are outlined in the following sections.

1.1. Overview on available EF approaches and elements

The EF was proved to be particularly efficient and accurate enough to simulate the nonlinear behaviour of structures dominated by a box-like behaviour, i.e., governed by the in-plane response of URM walls and characterized by effective wall-to-wall and wall—to-diaphragms connections [4,15–17,26].

Various nonlinear modelling approaches may be adopted for URM panels, as outlined in Ref. [2]. In this paper, two main modelling approaches are considered. The first approach is the lumped plasticity (LP). It may be built on the addition of zero-length hinges in three positions [2]: two flexural hinges at the ends of the edge and a shear-hinge usually at the centre of the edge (assumed as constant along the panel). This approach does not permit accounting for the coupling of the axial-flexural behaviour. Hence, it needs to be additionally set through simplified approaches based on phenomenological laws or experimental or empirical formulae. Nevertheless, it is the most common solution implemented in EF commercial software packages [25]. For example, software packages that adopt the LP approach are 3Muri (2016–2020) that refers to the scientific work proposed in Ref. [5]; Pro-SAM (2020), based on the solver developed by Ref. [27]; MIDAS Gen (2017) that uses an alternative formulation based on concentrated hinges or the fibre model proposed in Ref. [28], CDSWin (2016) [29]; or Aedes. PCM (2017), based on the hinge formulation proposed in Ref. [30].

The second approach is distributed plasticity (DP). Unlike the LP method, DP enables explicitly coping with the progressive degradation of the axial-flexural cracking. It can produce more accurate models but requires a higher computational cost. In Ref. [31], an EF DP-based mathematical model was proposed that could be used to model both URM and RC-infilled structures. In Ref. [32], a DP-based macro-element that added a shear hinge at the centre of the edge was developed within the Midas GEN software framework. A shear-distortion phenomenological law was defined, and a simple 2D masonry wall was analysed. There are some DP models that enable coupling the shear and the normal component as in Refs. [33,34]. However, their formulation is rather complex.

Some DP EF-elements were already developed in OpenSees [35], which is a specific open-source software for earthquake engineering problems. In Ref. [17], a 3D macro-element was proposed that coped with the in-plane and out-of-plane behaviour of masonry walls. It was analysed by means of experimental tests on a single-panel scale. In Ref. [36], a force-based DP frame model was developed

for OpenSees. The element formulation considered axial, bending and shear deformations within the framework of the Timoshenko beam theory. Nonlinear materials were applied to force-beam elements to describe the fibre behaviour. In addition, a shear phenomenological constitutive law was added at the centre of the element to account for the nonlinear shear behaviour of the element. Cyclic analyses were performed at a single-panel scale. The authors concluded that the model accuracy is strongly dependent on the integration scheme and the shear constitutive laws used. In Ref. [37], the element proposed in Ref. [36] was validated in the OpenSees framework by varying the fibre and the shear laws. A regular two-storey case study building was analysed through pseudo-static and dynamic experimental tests to validate the model. In Ref. [38], the same element was validated for irregular masonry walls by comparing the results obtained with FE analyses of panels. In Ref. [39], a macro-element based on the multiple-vertical-line-element-model (MVLEM) was developed in OpenSees. This element was originally developed and calibrated for RC walls. Therefore, it requires some assumptions to be applied to URM walls. Additionally, the MVLEM does not allow modelling horizontal elements, neglecting the contribution of the spandrels.

In general, the elements proposed in the OpenSees framework present certain limitations. First, they do not bear in mind the specific behaviour of spandrels, which can be significantly different than piers [40]. Spandrels present higher drift limits than piers, as they are affected by the interlocking phenomena, and they can affect the boundary conditions of piers (which can be of fixed-fixed or cantilever behaviour). Second, none of the works accounted for the contribution of lintels, arches or tie rods/RC beams to the strength of the spandrel elements. As suggested by Refs. [17,41], modelling horizontal elements can affect the global seismic behaviour of URM structures. Also, as shown in Ref. [42], these elements might play an important role, in particular, after cracking, i.e., for the residual strength. This effect is considered in the Italian NTC code. As suggested by Ref. [20], varying these parameters would significantly change the response of multi-storey masonry structures. Third, the authors stemmed drifts and shear limits from experience and from the American codes, but they did not consider the affection of these parameters in the global behaviour of the URM structures. Fourth, some works took into account the variation of the axial load in the strength of the panels [36,38,43] with a rather limited analysis of its possible effect. As highlighted by Ref. [24], it is one of the parameters that most affects the drift capacity of the walls.

1.2. Scope of this work

As concluded from the state-of-the-art review, different EF modelling approaches have been proposed and developed in commercial software for the specific assessment of masonry buildings. Such is the case of the 3Muri, adopted in this paper as representative of a larger set of EF models, and the LP approach. This paper focuses instead on the implementation of EF strategies in general-purposes source software, like OpenSees. In fact, some tricky issues as well as the advantages and the limitations in doing this ad hoc use of general-purposes packages have not yet been accurately compared nor analysed in the literature. Among the larger set of options available in OpenSees (some of which include also more refined macro-elements, like the one proposed in Ref. [17]), in this paper, only the lumped and the distributed strategies have been explored. That reflects the choice of using solutions more compatible with software packages used in the engineering practice than at research level.

To pursue this goal, this work is focused on comparing these EF modelling approaches in both the 3Muri and the OpenSees software to assess key aspects that affect the behaviour and the EF modelling of URM walls (horizontal elements, variation of axial load, phenomenological constitutive laws) [52–54]. Both the axial-flexural and the shear behaviours have been accounted for simulating the typical failure types in masonry walls: the rocking and the crushing failures, and the diagonal cracking, respectively. Some benchmark structures proposed in the '*URM nonlinear modelling* – Benchmark project' (in the following, "benchmark project" for sake of brevity) has been adopted as first reference to validate the reliability of achievable results. Such structures consist of some single panels and a trilith. In such project, the results of various software packages were already compared and presented in an anonymous format, since

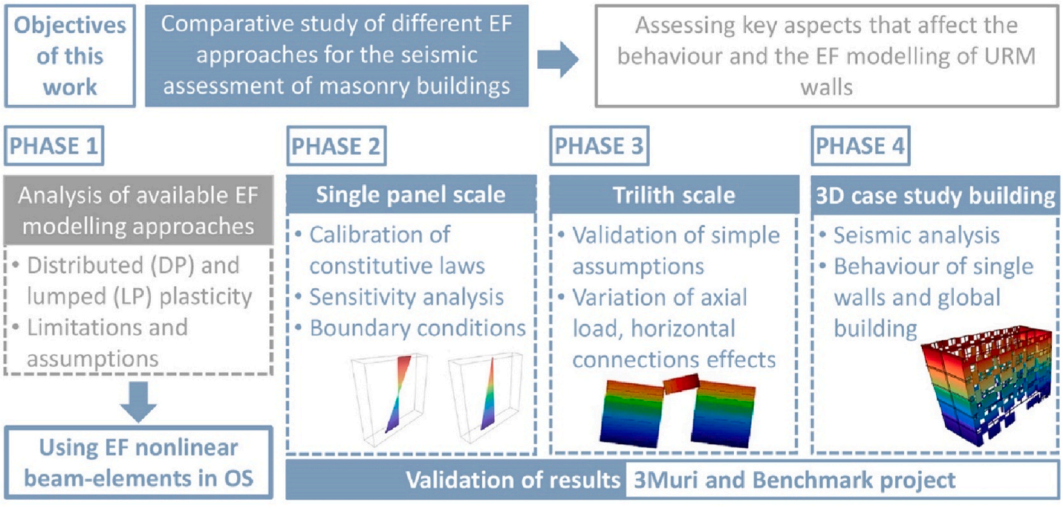

Fig. 1. Flowchart of the research work.

the goal was not to express a judgment on each single software but to compare the results of various tools when used under consistent hypotheses and evaluate the potential scatter on the base shear, stiffness, ductility of pushover curves, etc. In this project, results of 3Muri were already founded in substantial agreement with the other ones. In this paper, conversely, only the results achievable with 3Muri are discussed, by assuming this tool as representative of a larger stock of commercial software package based on the EF strategy. This assumption is considered licit since in the works already mentioned of this project [21,22], it has been investigated that - under consistent hypotheses – they are able to obtain results with a limited scatter even in the case of much more complex systems, representative of 3D buildings.

A flowchart of the work developed is shown in Fig. 1. In §1, a brief introduction to the problem and analysis of the state of the art is presented. In §2, the EF approaches considered are presented as well as the corresponding constitutive models and the target behaviour for the calibration (Phase 1). In §3, a comparison of the modelling approaches is shown for the calibration of the constitutive laws considering a single panel (Phase 2). In §4, the validation of the simple assumptions is carried out on a basic frame (trilith) scale (Phase 3). In §5, the seismic analysis of a case study building is performed in 3D to obtain and to compare the behaviour of a real complex system considering each approach (Phase 4). This 3D structure has been selected to be representative of the existing URM building stock in Seville, which the future developments of this research will be addressed to. In §6, the conclusions and the future work are presented.

2. Equivalent frame approaches

2.1. Description of non-linear elements adopted in OS

Both piers and spandrels (Fig. 2) are conceived as non-linear beam models that can accurately account for the main failure modes of the walls.

The failure mechanisms of masonry piers subjected to horizontal loads (seismic) are divided into two main classes, i.e., flexural and shear (Fig. 3). The first is related to the rocking and the crushing failures and can be captured by simulating the axial load-bending moment (*N-M*) response. The second is linked to the diagonal cracking failure and it can be simulated through shear force-deformation/displacement (V-γ) (even multi-linear as adopted in Ref. [15]) or (V-d) laws. As already introduced, in this work, the elements have been modelled following two plasticity approaches: the DP and LP. The method presented in Ref. [5] for the EF idealisation of URM walls has been followed to adopt consistent assumption in the geometry of panels.

Three elements have been used as available in OpenSees, as shown in Fig. 4. Considering the DP, two elements have been adopted: the distributed plasticity modelled in deformation (strain) (DP-DF) and the distributed plasticity modelled in displacement (DP-DI).

The DP-DF consists of a force-based element (FBE) with fibre cross-sections as in Refs. [36,38,43]. The element is able to capture the axial-flexural behaviour through the fibre sections to predict the in-plane and the out-of-plane behaviour. The element is based on the Timoshenko beam theory in which sections remain plane after deformation. Gauss-Lobatto points are defined. To account for the bending failure, two points at the ends of the edges have been added. To account for the shear, one integration point has been added as aggregator. Masonry nonlinearity is simulated by means of a nonlinear uniaxial stress-strain (σ-ε) law along the frame [44]. The uniaxial material 'Concrete06' available in OpenSees has been used [45]. Although this material was originally proposed for concrete, it has been proved to satisfactorily capture the masonry behaviour [43]. In fact, this material considers both the compression and the tensile strengths, reproducing a more accurate masonry behaviour. Also, it enables accounting for the softening branch of masonries. The softening has been computed according to Refs. [36,45] and considering the shape factors defined in Ref. [36]. In this case, n, k and b are equal to 2, 1 and 4, respectively. A phenomenological shear force-deformation (V-γ) law has been defined to account for the shear using the 'pinching4' uniaxial material available in OpenSees. This command is commonly used to construct a uniaxial material that represents a 'pinched' load-deformation response and exhibits degradation under cyclic loading. It requires several parameters for the negative (n) and the positive (p) responses of the curve. Additional parameters are needed for the unloading-reloading behaviour and the hysteretic damage. The 'section-aggregator' command is used to couple the flexural and the shear behaviours. The DP-DI is based on the previous DP-DF. It has been specifically developed in the STKO software [46], which is a pre- and post-processor specifically conceived for OpenSees. The shear behaviour is captured by a shear force-displacement relationship (V-d) and the 'Beam With Shear Hinge Property' is used to apply the shear hinge. Since it includes an additional section at the middle of the edges, it can enable higher accuracy. The 'rigidbeam' constrain type has been applied to simulate the rigid elements that connect piers and spandrels. The

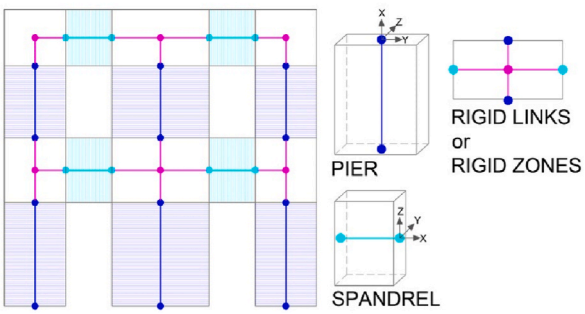

Fig. 2. Equivalent frame idealisation.

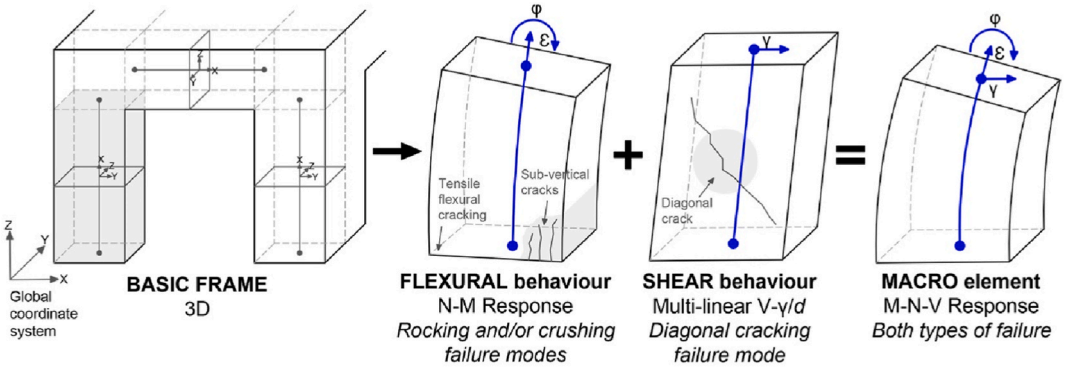

Fig. 3. Macro-element behaviour.

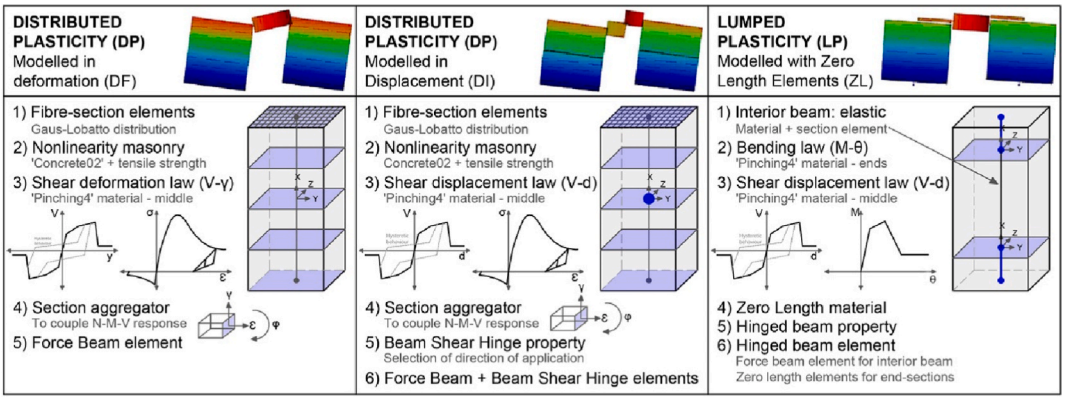

Fig. 4. EF nonlinear beam-elements considered in the analyses.

results obtained from OpenSees have been handled in the STKO software.

The third element used in OpenSees is based on the LP approach; this is the more similar to the one implemented in 3Muri. It is an FBE with zero-length hinges: two bending hinges located at the end of the edge and one shear hinge at the centre. As proposed in previous works [36,38,43,47], the interior beam is elastic, modelled with the 'Elastic' uniaxial material. A *V-d* law has also been defined with the 'pinching4' material to account for shear. For this model, a bending-moment (*M-θ*) law has been defined to enable the coupling of the axial-flexural behaviour. It has been implemented using the 'pinching4' material. Additional information regarding the calibration of the constitutive laws is presented in the following section for each element.

2.2. Target behaviour for the calibration

The drift limits and some strength criteria already proposed in the literature [23] have been assumed as input data to describe the main failure modes. Indeed, each seismic code considers different criteria to account for the flexural and the shear behaviour of EF masonry panels [23]. In this work, they are defined according to the Italian NTC code [48] and consistently with the benchmark project assumptions [25] (Table 1).

The flexural behaviour in the DP models has been accounted for through the nonlinear uniaxial σ-ε law along the frame using 'Concrete06' uniaxial material available in OpenSees (Fig. 5(a)). The compression curve is described in Eq. (1), as suggested by

Table 1
Strength criteria adopted in this work for piers and spandrels.

FAILURE	PIERS	SPANDRELS
Flexural failure	$M_u = \frac{\sigma_0 l^2 t}{2}\left(1 - \frac{\sigma_0}{0.85 f_{md}}\right)$	$M_u = H_p \frac{h}{2}\left(1 - \frac{H_p}{0.85 f_{hd} h t}\right)$
	$V_u^{PF} = \frac{M_u}{h_0}$ *Cantilever* $\rightarrow h_0 = h_{eff}$	$V_u^{PF} = \frac{2M_u}{l_{eff}}$
	Fixed − *fixed* $\rightarrow h_0 = h_{eff}/2$	$H_p = min(A_s F_{ym}; 0.4 f_{hd} t l)$
Diagonal cracking	$V_t = \frac{1.5\tau_{0d} l t}{\beta}\sqrt{1 + \frac{\sigma_0}{1.5\tau_{0d}}}$ with β coefficient function of the element slenderness, equal to: 1 if $h_{eff}/l < 1$; h_{eff}/l if $1 \leq h_{eff}/l \leq 1.5$; 1.5 if $h_{eff}/l > 1.5$	$V_t = \frac{1.5\tau_0 l t}{\beta}\sqrt{1 + \frac{\sigma_0}{1.5\tau_0}}$

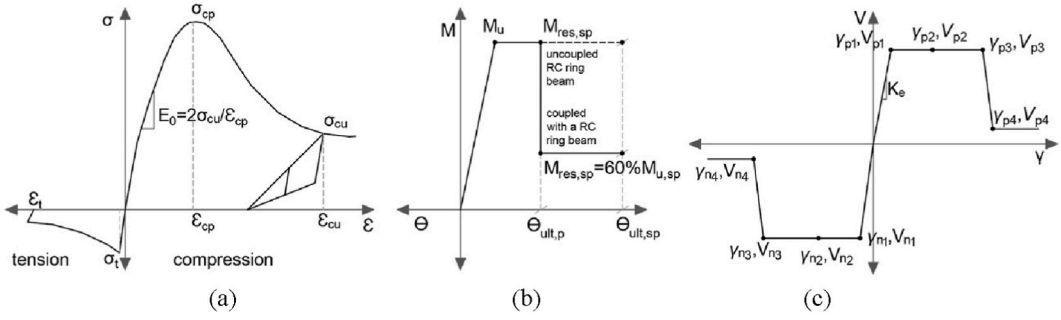

Fig. 5. Constitutive laws: (a) nonlinear uniaxial σ-ε material using 'Concrete06' for the DP-based approaches; (b) M-θ law for the LP approach; (c) V-γ law to account for shear in all the modelling approaches.

Ref. [36]. The tensile behaviour has been simulated following the equations proposed by Ref. [49] by dividing the curve into two branches (Eq. (2) and (3)). The calibration of the parameters is performed in §3 through a parametric analysis on a single panel scale.

$$compression\ domain: \sigma_c = f_{md}\frac{n\left(\varepsilon_c/\varepsilon_{cp}\right)}{n-1+\left(\varepsilon_c/\varepsilon_{cp}\right)^{nk}} \tag{1}$$

$$tensile\ domain\left(\varepsilon_t \le \varepsilon_{tp}\right): \sigma_t = \left(f_{td}/\varepsilon_{tp}\right)\varepsilon_m \tag{2}$$

$$tensile\ domain\ \left(\varepsilon_t > \varepsilon_{tp}\right): \sigma_t = f_{td}\left(\varepsilon_{tp}/\varepsilon_t\right)^b \tag{3}$$

Where σ_c and σ_t are the stress values in the compression and tensile domain; ϵ_c and ϵ_t are the strain values in the compression and tensile domain; n is the compressive shape factor and k is the post-peak compressive shape factor, both defined according to Ref. [36]; and b is a constant input parameter defined from Ref. [36].

For the LP approach, the flexural behaviour of both piers and spandrels has been simulated by defining a M-θ curve through two approaches: i) empirical (E), from the M-θ law computed for each panel from the DP-DF model; and ii) analytical (A), from a phenomenological law (Fig. 5(b)). For the analytical, the flexural response has been assigned to piers following the prescriptions described in Ref. [50]. However, the ultimate bending moment of piers ($M_{u,p}$) has been calculated according to Table 1. In the case of spandrels, the flexural response has been interpreted to account for the contribution of the equivalent tensile strength. As concluded by Ref. [40], there is a sudden decay of the strength of spandrels associated with their flexural cracking. This was computed as 60% of the strength when the spandrel is coupled to an RC beam or lintel. No reduction was considered if it is not coupled with an RC element. The ultimate bending moment of spandrels ($M_{u,sp}$) is calculated according to Table 1. Regarding drifts, in the case of piers, the ultimate drift ($\theta_{ult,p}$) has been equal to 0.005%, to account for the flexural/bed joint sliding in regular masonry piers. In the case of spandrels, the $\theta_{ult,sp}$ has been increased up to 0.02%, given the experimental results obtained in Ref. [51] for spandrels coupled with tensile elements. The criterion consistent with the Turnšek and Čačovič (T&C) failure [52] has been used to estimate the shear strength of URM panels as shown in Table 1, following the benchmark criteria.

The simulation of the shear behaviour has been achieved by calibrating V-γ or V-d constitutive laws associated with the nonlinear hinges located at the centre of the EF-elements. Each point of the law (Fig. 5(c)) has been defined according to mechanical criteria and the experimental scientific literature. The ultimate shear strength, V_3, has been calculated in line with the T&C criterion. The ultimate deformation, γ_3, has been set to 0.4%, as suggested by several works and codes [11,53]. The initial diagonal cracking shear, V_1, and the middle value, V_2, have remained equal to V_3. Following the prescriptions of the NTC-18, the shear deformation at the initial elastic branch, γ_1, has been computed as V_3/K_e, where K_e is the wall initial elastic shear stiffness computed as Eq. (4). In order to account for the cracked stiffness, a conventional reduction of 50% of the elastic stiffness properties has been considered, as in Ref. [5], by defining k_2 as 0.5. An average value of γ_2 has been assumed as $(\gamma_1 + \gamma_3)/2$. The description of the post-peak response of masonry panels subjected to shear is challenging since it depends on many factors [36]. In this case, V_4 has been assumed as 20% of V_3 and γ_4 has been set as 1%, as suggested by the FEMA-356 and [32].

$$K_e = \left(\frac{h^3}{k_1 k_2 EJ} + \frac{h}{k_2 G A_v}\right)^{-1} \tag{4}$$

Where k_1 is a coefficient that depends on the boundary conditions of the panels: 12 and 3 for the fixed-fixed and cantilever conditions, respectively; A_v is the area of the of the transversal section divided by 1.2; J is the moment of inertia of the transversal section of the panel; E and G are the Young's modulus and the shear modulus of the panel; and k_2 is a coefficient to account for the cracking degradation.

2.3. Limitations

The acting axial load (N) in panels changes during the analyses due to the redistribution of vertical loads derived from the application of horizontal loads. As a consequence, the value of the shear strength in each panel varies during the NLS analysis [5]. In 3Muri, the redistribution is automatically calculated, and the strength consequently updated at each step of the analysis. However, this automatization has not yet been implemented in OpenSees, in which the properties of plastic hinges are defined at the beginning of the analysis on basis of the gravity loads. Thus, in this work, the effects of the variation of the axial load have been analysed to obtain an insight concerning how this variation could affect the global behaviour of a case study building in 3D.

3. Analysis at single panel scale – comparison of results

3.1. Parameters considered in the sensitivity analysis

In this section, the results obtained on a single panel scale are presented to study the influence of the mechanical parameters. The sample configuration (Fig. 6), the mechanical properties (Table 2) and the results, all coming from the structure nº2 proposed in the benchmark project, are used to perform and to validate the analyses [25]. A sensitivity analysis has been carried out to obtain the main parameters that affect the constitutive law of the DP-based models. The masonry compressive strength (f_{cm}) (given value from the benchmark) has been set at the beginning of analyses and the five different mechanical parameters needed to define the 'Concrete06' uniaxial material have been varied (marked in red in Fig. 7): the strain at peak compressive stress, ε_{cp}; the masonry compressive crushing strength, f_{cu}; the strain at f_{cu}, ε_{cu}; the masonry tensile strength, f_t; and the strain at peak tensile strength, ε_{tp}.

In order to define the variation range of each parameter, an analysis of different results of experimental tests on masonry walls has been performed (Table 3). Two types of ceramic bricks have been considered: solid, used in the analyses of the benchmark project; and horizontal hollow, used for the case study analysis. Considering the variation ranges of the solid bricks, three different constitutive models have been set (Table 4): A, brittle behaviour; B, medium; and C, more ductile behaviour. Finally, the B* constitutive model has been defined after performing the parametric analysis on the mechanical properties of the constitutive laws. B* has been selected since it best matched the strength criteria available in the literature and also adopted as reference in the benchmark project.

3.2. Results obtained from the sensitivity analysis

In Fig. 8(a), the shear behaviour has been neglected to check whether the model was able to capture the flexural behaviour properly. These plots are expressed as the ratio σ/f_{cm} vs the total shear force at the base of the panel (V_b). It can be observed that the model highly matches the strength domains for each of the possible boundary conditions of piers (fixed-fixed (FF) or cantilever (CA)) for the same constitutive model B. This constitutive model has been checked as an average model to verify whether OpenSees is capable of properly reproducing the boundary conditions. Next, different constitutive laws have been analysed and, among them, the B constitutive law has better captured the prescribed flexural behaviour. At lower ratios of σ/f_{cm}, the panel is governed by the tensile behaviour: it does not tend to be 0. Therefore, a specific analysis of the importance of the tensile strength has been performed by varying the constitutive models. In this case, the tensile behaviour of both A (tenA) and C (tenC) models have been combined with the compressive behaviour of model B. As can be observed, for lower ratios of σ/f_{cm}, laws with lower values of tensile strength can fit better the strength domain. However, for higher ratios of σ/f_{cm}, the slope of the curve was higher and the results did not match the strength curve. Therefore, in order to fit the results, an additional B* constitutive law has been defined. It presented lower values of strains and tensile strength. Regarding the shear behaviour, τ_0 has been modified for each of the constitutive models considered and the corresponding T&C diagonal cracking curve. In Fig. 8(b), it can be observed that the results highly match its corresponding T&C curve with a disruption at lower ratios of σ/f_{cm}. In OpenSees, all vertical and horizontal NLS analyses have been performed by means of the load- and the displacement-control integrator, respectively. In 3Muri, a specific algorithm has been implemented to manage NLS analyses by imposing increasing displacements under a given horizontal load pattern (see Ref. [5] for further information).

In Fig. 9(a), the constitutive law has been varied while τ_0 remained constant, concluding that the shear behaviour mainly depends on the diagonal cracking strength. In Fig. 9(b), the effect of the axial load on the shear hinge properties has been analysed. Three situations have been set considering the B* constitutive law: setting fixed the axial load of the shear property to 160 kN (setSH) and 800 kN while varying the axial load acting on the panel ('setSH'); and, varying both the axial load of the shear hinge and acting on the panel ('nosetSH'). It can be seen that for smaller ratios of σ/f_{cm}, the model is able to capture the target behaviour remaining shear. However, for higher ratios of σ/f_{cm}, the model is not able to simulate the expected behaviour. Therefore, if the shear hinge properties

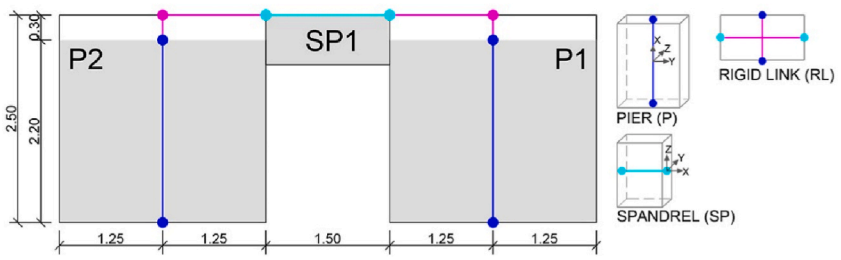

Fig. 6. Sample model BS.2 from the '*URM nonlinear modelling* – Benchmark project'.

Table 2
Masonry mechanical parameters used in the benchmark project.

Masonry	$f_{cm} = 2.7$ MPa	$\tau_0 = 0.054$ MPa	$E = 1450$ MPa	$G = 483$ MPa	$W = 21$kN/m3

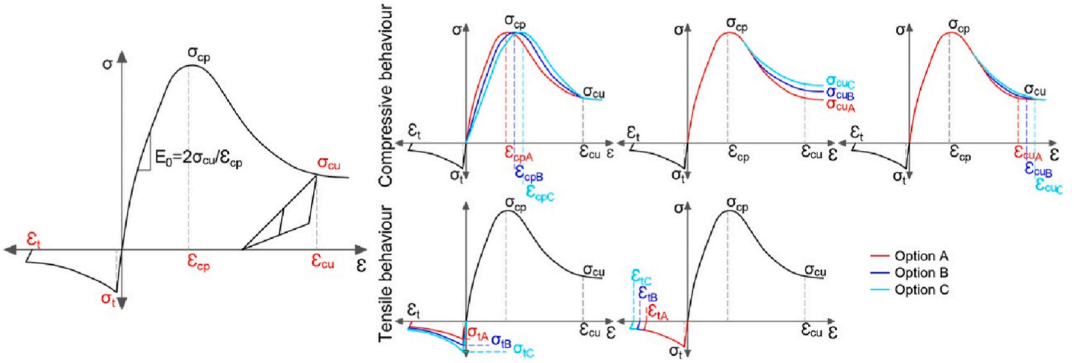

Fig. 7. Mechanical parameters varied in the parametric analysis.

are not updated during the analyses, at higher ratios of σ/f_{cm}, the results might not be reliable. Additionally, in Fig. 9(c), the influence of the application of the axial load (gravitational loads and self-weight of the URM panel) has been analysed considering two methods: a concentrated load (Con) at the upper node and distributed (Dist) along the edge. It has been obtained that the results were similar despite the method of application. Thus, it has been decided to apply the loads concentrated in nodes as in 3Muri.

The results of the NLS analyses varying N in the shear properties as well as the acting vertical load in panels are plotted in Fig. 10, computing the displacement at the top of the panel (d_{top}). The maximum values of the shear strength at the base (V_b) are similar to those obtained by 3Muri. They range from: $N = 160$ kN, $V_b = 132$–153 kN; $N = 400$ kN, $V_b = 160$–192 kN; and $N = 600$ kN, $V_b = 231$–232 kN. It can be observed that the LP-based models are more capable of capturing a similar stiffness as in 3Muri. In the case of DP-based models, they are not as capable as the LP models of capturing the same stiffness as in 3Muri. This is worse even or higher values of N. This is due to the difficulty to account for the degradation of the flexural behaviour in DP-based models.

4. Analysis at the trilith scale – comparison of results

In this section, the results obtained on a trilith scale (Fig. 6) are presented to validate simple assumptions. The sample model BS.2 from the benchmark project has been reproduced. As stated, the strength in panels depends on the variation of N during the NLS analysis. Consequently, the global behaviour of the structure may vary. In this work, the variation of the acting N in the benchmark panels with and without an RC ring beam has been studied and presented in Fig. 11. As it can be seen, there is a redistribution of the acting N in panels up to a certain level of deformation ($\theta = 0.16\%$, which corresponds a displacement of the top of 4 mm). The variation of N is slightly higher in OpenSees than in 3Muri. If a RC ring beam is considered, the variation is higher in all the models. The shear hinge governs the behaviour of panels for higher ratios of σ/f_{cm} as previously observed in Fig. 8. If panels are governed by flexural behaviour, the models are capable of reproducing the failure properly in both software. In OS, this is possible thanks to the ZL elements and the section aggregator. The effect of the variation of N into strength and failure modes prediction is automatically calculated in 3Muri, however, in OS, this is not possible. Therefore, if the variation of N produces a transition to the diagonal cracking failure, further analyses are then needed in OpenSees to properly account for it.

Various effective lengths of RC ring beams may be considered in 3Muri, by acting on the value of R parameter (Fig. 12); these different effective lengths reflect the possibility of having in the reality a difference effectiveness of confinement provided by masonry to RC elements. In order to propose consistent models in OS, an analysis of the effects of each possible configuration in 3Muri is carried out. In Fig. 13, the results of NLS analyses of the trilith are presented considering the global and the single piers scale behaviours. As can be observed, the global behaviour of this simple structure is not affected by varying the length of the ring beam. However, at panel scale, the increase of the length of the ring beam leads to higher values of initial stiffness by up to 5%. For analyses carried out in §5, it has been opted to define the length of the ring beam as the spandrel's length in both software (R = 0).

NLS analyses (setting N as 160 kN) have been performed to determine the global capacity curves of the trilith, with (Fig. 14(a)) and without (Fig. 14(b)) RC ring beams. The results attained in OpenSees are rather similar to those obtained in 3Muri. The LP-E model, based on the lumped plasticity approach and using an empirical formulation for the flexural behaviour, obtained worse results than the others. This is due to the lack of consistency when computing the M-θ law to define the flexural behaviour. Therefore, due to its poor results, it has been opted to omit this configuration during the rest of the work. If ring beams are borne in mind, better results are obtained. In fact, the LP-A approach presents similar values to 3Muri since it tends to reproduce the same modelling procedure in OpenSees. The DP-based approaches obtained rather similar results to 3Muri, achieving minor differences when computing the initial stiffness of the system.

Table 3
Mechanical properties of nonlinear behaviour of ceramic brick masonry walls.

Brick type	Works	E [GPa]	G [GPa]	W [kN/m^3]	c [MPa]	μ [−]	f_{cm} [MPa]	ε_{cp} [−]	ε_{cu} [−]	f_t [MPa]	ε_t [−]	τ_0 [MPa]
Solid	[32]	1.49					6.2	0.0009		0.18	1.8e^{-05}	0.12
	[36]	0.87	0.23	19		0.4	1			0.1		0.067
	[54]	2.46	1.13				3.28			0.15		0.1
	[55]				0.23	0.58	6.2	0.0009		0.18	1.8e^{-05}	0.12
	[56]						6.2 ± 12%					
	[57]										1.3e^{-05}	0.69
	[10]	1.50	0.50	18			3.2			0.114		0.76
	[47]	4.25	1.00	18			6					
	[37]	2.53	0.84				3.28			0.14		0.093
	[20]						5–6.2	0–0.003	0.008–0.012	0.15–0.35	0.0005–0.02	
	[40]					0.58	6.2			0.122		
	[53]				0.21	0.81	7.9 ± 20%					
Hollow	[58]	1.69					1.6					
	[59]	3.5–5.6	0.87–1.4	15			4–8			0.2–0.36		0.18–0.60
	[11]	1.12–1.4										

Table 4
Assumed range of variation of uniaxial stress-strain constitutive laws.

Option	ε_{cp} [−]	f_{cu} [kPa]	ε_{cu} [−]	f_t [kPa]	ε_t [−]	E_0 [GPa]
A	0.00048	15%f_{cm}	0.0064	2% $f_c = 1/50$	0.00016	11,111
B	0.0008	20%f_{cm}	0.008	4% $f_c = 1/25$	0.0005	6666
C	0.00112	25%f_{cm}	0.0096	6% $f_c = 1/16$	0.001	4761
B*	0.0008	22%f_{cm}	0.008	5% f_c	0.005	1760

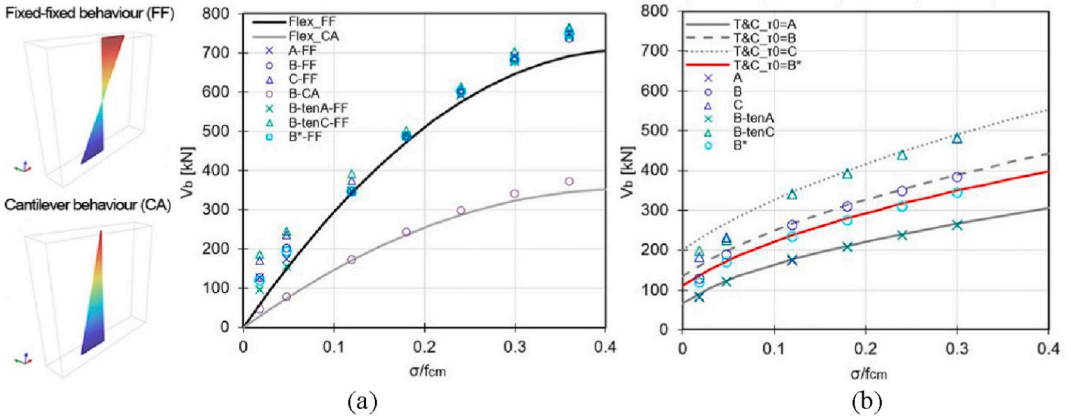

Fig. 8. (a) Simulation of the flexural behaviour and the affection of the boundary conditions in piers. (b) Simulation of the shear behaviour in piers.

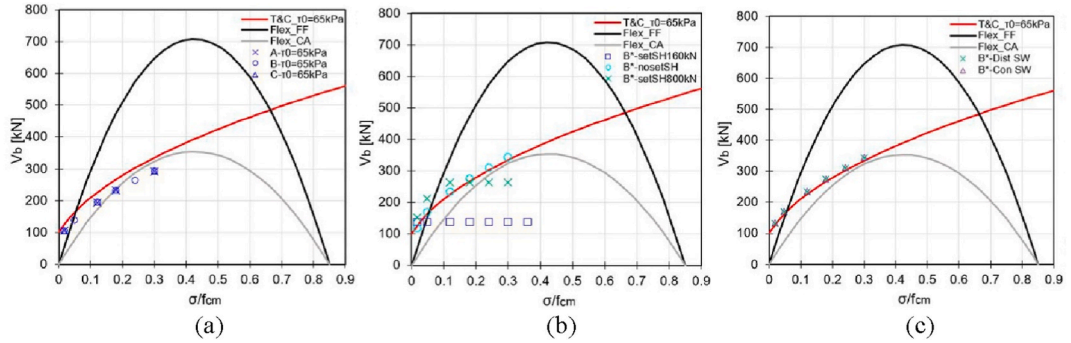

Fig. 9. (a) Analysis of the effects of τ_0. (b) Effects of varying the axial load in the shear hinge properties. (c) Application of the axial loads the in models.

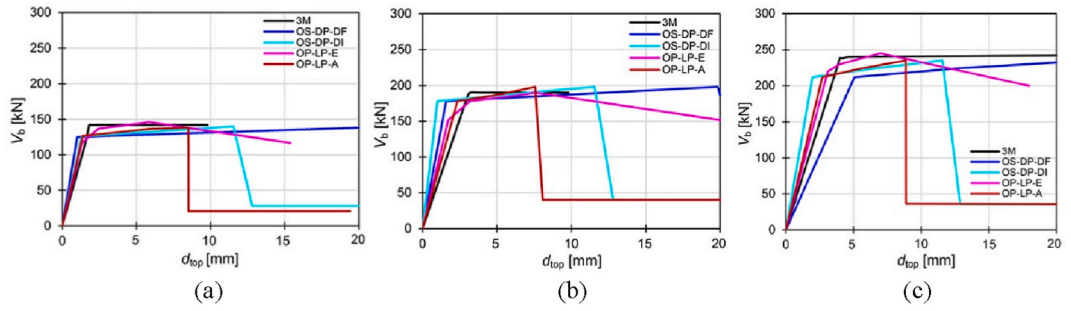

Fig. 10. Capacity curves of a single pier varying the value of N in shear hinge properties and acting vertical load: (a) $N = 160$ kN, (b) $N = 400$ kN, (c) $N = 600$ kN.

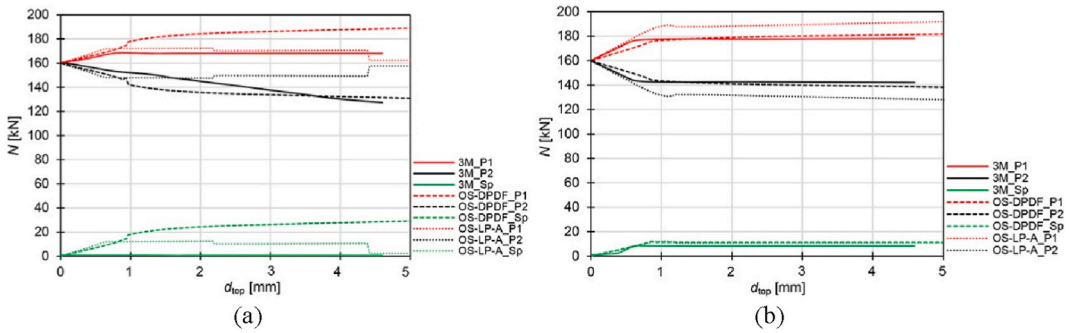

Fig. 11. Variation of the axial load acting in panels (a) without and (b) with an RC ring beam.

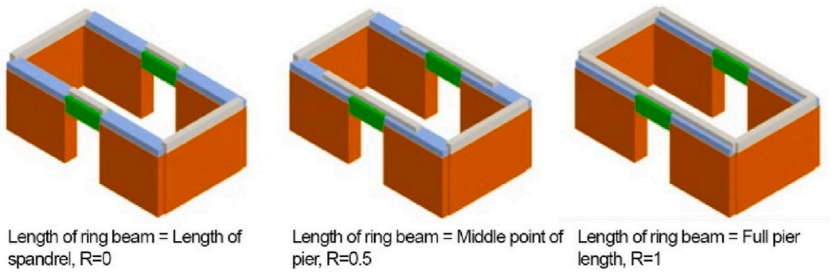

Fig. 12. Configuration of RC ring beam in 3 M and value of R.

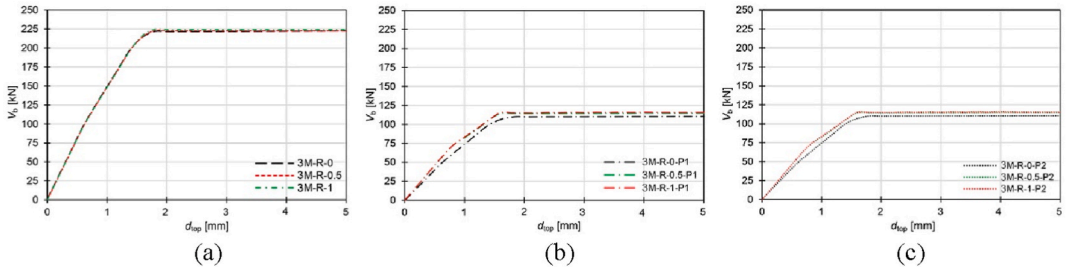

Fig. 13. Capacity curves of the trilith varying the ring beam dimensions in 3Muri (3 M). (a) Global behaviour, (b) single P1; and (c) single P2.

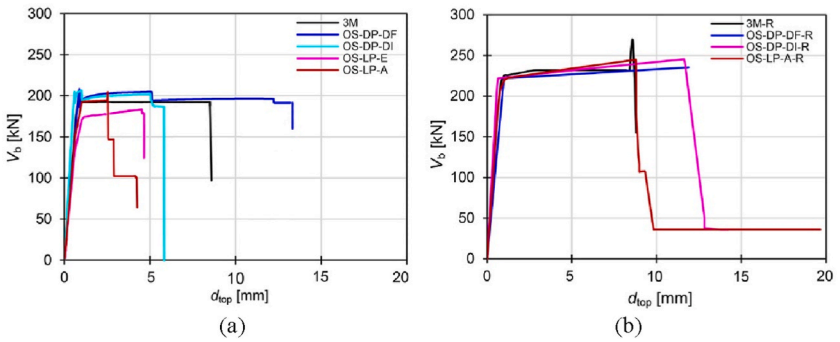

Fig. 14. Capacity curves of the trilith (a) without (plotting all the curves obtained in the benchmark project for the same model using different software packages) and (b) with an RC ring beam.

Fig. 15. Situation of the neighbourhood of 'El Plantinar' in Seville (Spain) and identification of block types.

5. Modelling and analysis of a pre-code masonry building in Spain

In this section, the EF modelling is extended to a real case study URM building representative of a more complex 3D system.

5.1. Case study description

The case study building is located in an old neighbourhood in Seville (Spain) called 'El Plantinar' (Fig. 15). It was constructed during the 1960s and before the application of seismic codes. Note that the first seismic code in force in Spain was published in 1969. The neighbourhood is composed of three different types of structural blocks. In some cases, the structures are connected and in others they are divided by structural joints. They all present a similar structural configuration: a mixed structure with URM walls in the perimeter and an RC frame with beams and columns in the centre of the plan. In this work, block Type 1 has been selected to be analysed. This is the largest one and can be found isolated, which enables avoiding the possible effects of pounding between adjacent buildings in seismic analyses [60].

The case study Type 1 is a 5-storey building constructed with URM walls whose thickness varies with height: 0.37 m on the ground floor and 0.24 m on the rest others. The walls were constructed with hollow, 5 × 11.5 × 24 cm ceramic bricks. The building presents ribbed slabs with pre-stressed, 0.25 m thick concrete joists and ceramic vaults. The slabs present a superficial layer of 0.04 m thick concrete and rebar, which guarantees its rigid behaviour. The system also has a narrow, 8 cm thick RC ring beam. The mechanical parameters, listed in Table 5, have been defined according to the analysis of reference experimental tests on hollow ceramic bricks (Table 3). The characteristic compressive strength, f_k, has been defined through the empirical equation established in Eurocode-6 (EC-6) (Eq. (5)) [61]. K is a constant that depends on the brick and mortar listed in the EC-6. In this case, for cooked clay and ordinary mortar, it is computed as 0.35. The specific weight has been selected in line with the construction code of application of this period, the Spanish MV-201 [62]. The structural configuration, the elevation and the constructive and structural details are depicted in Fig. 16.

$$f_k = K f_b^{0.7} f_m^{0.3} \tag{5}$$

5.2. Numerical modelling

In order to be consistent as much as possible in the modelling assumptions, the EF idealisation in OpenSees has been carried out according to the geometry of panels proposed by 3Muri (Fig. 17), according to the rules described in Ref. [5]. The adoption of such rules appears quite reasonable in this case, which is characterized by a quite regular layout of openings; in other literature works, the effect of such epistemic uncertainty has been investigated [21]. Also, the loads and the masses acting in each panel have been assumed

Table 5
Assumed mechanical parameters after the analysis of the state of the art in Table 3.

Masonry	$W = 18$ kN/m^3	$f_{cm} = 4.0$ MPa	$f_{ck} = 1.14$ MPa	$E = 1.200$ GPa	$G = 0.15$ GPa
		$f_b = 3$ MPa	$f_m = 4$ MPa	$\tau_0 = 0.05$ MPa	
RC	$W = 25$ kN/m^3	$f_{c\text{-}rc} = 25.5$ MPa	$f_{ck} = 17.5$ MPa	$E = 30$ GPa	$G = 12$ GPa
Steel	$W = 78.6$ kN/m^3	$f_y = 428$ MPa	$f_{yk} = 400$ MPa	$E = 210$ GPa	$G = 80$ GPa

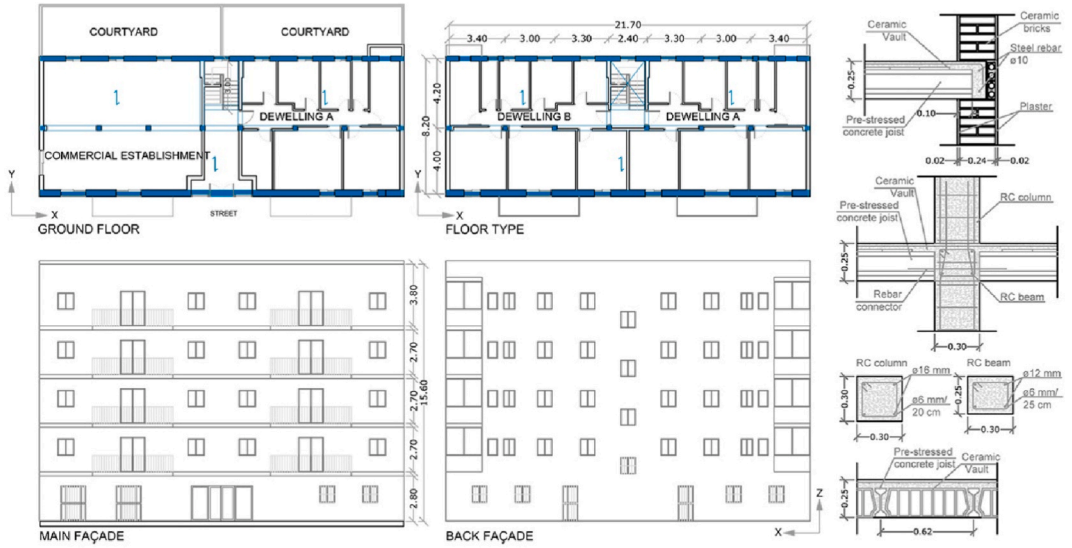

Fig. 16. Structural configuration. Distribution in plan and elevation. Constructive and structural details.

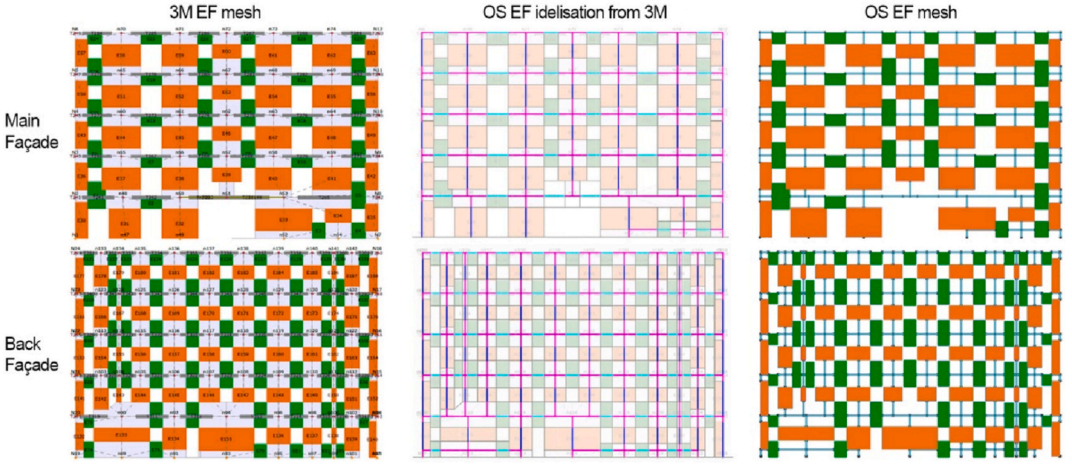

Fig. 17. EF mesh idealisation for each façade in each software package.

in OpenSees model consistently with the 3Muri one. The case study building has been modelled in OpenSees following the DP-DF, the DP-DI and the LP-ZL-A approaches. In order to make negligible the influence of the called "flange effect" (that may intervene at the intersection of connected piers), a 5 cm long steel beam has been added in the corners of the structure and in each floor. Moreover, the initial *N* acting in panels has been set at the beginning of the analysis according to the results from the gravitational loads computed in 3Muri. The structures have been fixed at the base. The RC interior frame has been modelled following the distributed plasticity approach as in Ref. [63]. For that, the 'nonlinearBeamColumn' elements have been used along the length of the RC members. 'Concrete02' and 'Steel02' uniaxial materials have been considered to simulate the nonlinear behaviour of the RC elements. The Mander-Priestley model has been followed to account for the confinement of the RC elements. Moreover, RC elements have been linked to the structure with 'EqDOF' constrains.

5.3. Results of the modal analyses

Similar values of periods have been obtained for the models as shown in Table 6. However, in the case of Mode 3, a higher period has been obtained for the 3Muri model compared to the rest of the OpenSees models. In order to compare the results achieved from the modal analysis carried out by the two software packages, the MAC procedure based on the Modal Assurance Criterion (MAC) index [64] has been used. This measures the similarity between the estimated mode shape vectors from the "reference" model and the ones compared. Values close to 1 indicate a good agreement between models. This approach is usually adopted to compare experimental (i.e. data from ambient measurement tests) and numerical data with the main goal to calibrate numerical models. In this case, instead the MAC values are used to quantify the differences between different models. It has been obtained that, for all four models, Modes 1 and 2

Table 6
Fundamental period (T) of vibration of the models.

Mode	Parameters	3 M	OS-DP-DF	OS-DP-DI	OS-LP-A
First Mode	Periods (s)	0.58	0.60	0.61	0.57
Second Mode	Periods (s)	0.44	0.37	0.48	0.42
Third Mode	Periods (s)	0.22	0.12	0.15	0.18

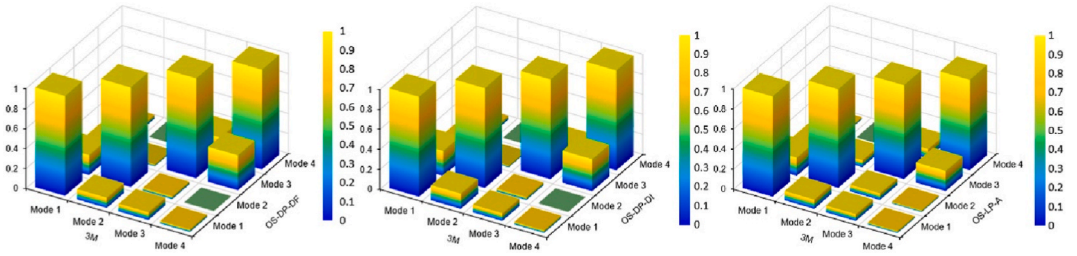

Fig. 18. Comparison of reference 3Muri (3 M) and OpenSees models vibrational modes in MAC index terms.

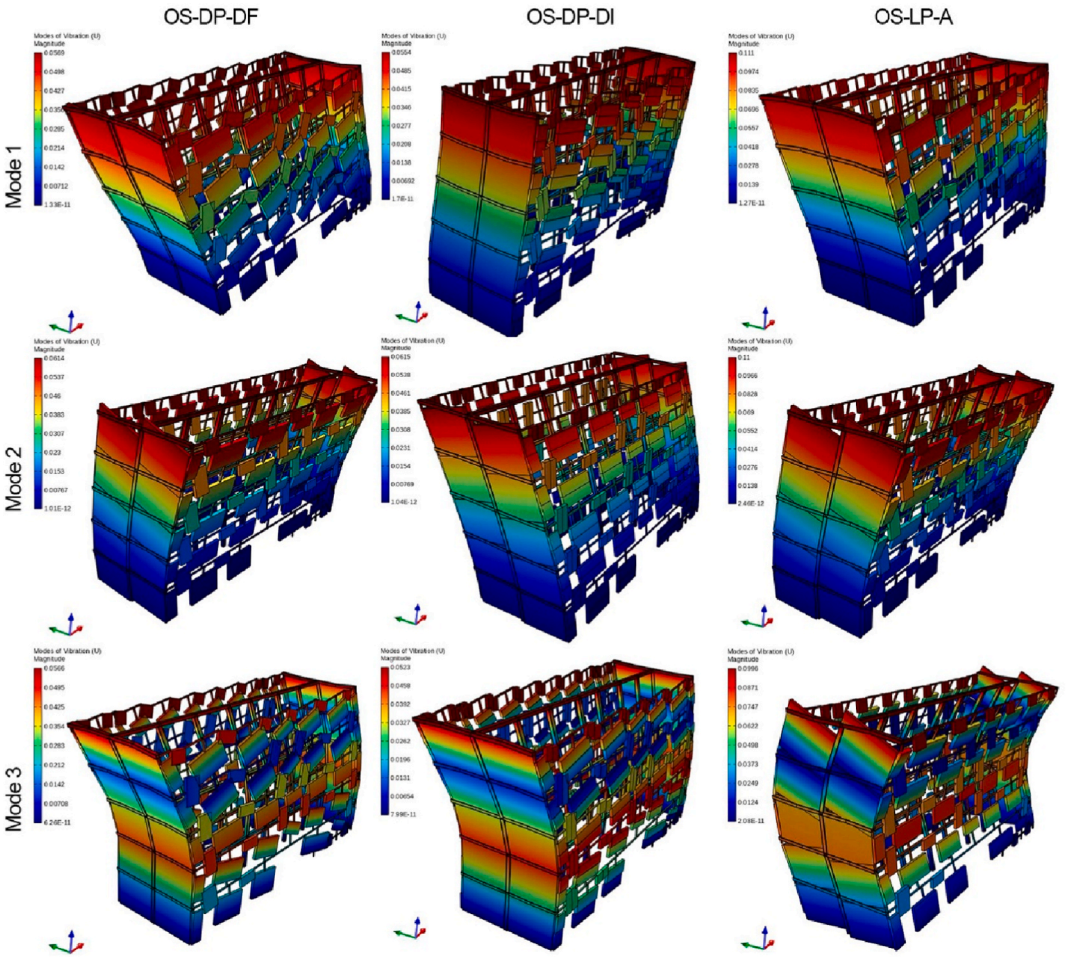

Fig. 19. Modal shapes of OpenSees models. X-direction, red axis. Y-direction, green axis. (For interpretation of the references to colour in this figure legend, the reader is referred to the Web version of this article.)

are translational in the X- and Y-directions, respectively. In Fig. 18, the results of the MAC procedure applied to each of the models considered are shown. It can be observed that a good prediction is obtained (values close to 1 in the diagonal). Nevertheless, some discrepancies have been obtained for Mode 3, which is related to the differences in the value of the period obtained with 3Muri.

In Fig. 19, the results of the modal shapes for OpenSees models have been shown. In the case of Mode 1, the modal participation factor ranges from 68.57% to 70.11%. However, in the case of Mode 2, the mass participation can be higher, from 68.66% to 76.29%. Mode 3 seems associated to a second mode shape for walls oriented along the Y direction combined with torsion.

5.4. Results of the nonlinear analyses

5.4.1. Walls behaviour

NLS analyses have been performed to obtain the pushover curves of each of the URM walls of the building for the uniform load pattern (Fig. 20). Additionally, the effects of the ring beam (R) have been assessed by considering (dotted lines) and not considering it (solid lines); pushover curves refer to the response of two main façades. It can be observed that the main façade wall presents a higher seismic capacity than the back's façade. The OpenSees models based on the LP approach, using the analytical formulae (OS-LP-A), is the one that reproduces better the behaviour computed in 3Muri. This is due to its capability of capturing the initial cracked stiffness compared to the DP-based approaches. In LP-models, the cracked stiffness can be considered in both the shear and flexural laws: *M-θ* and *V-d* laws. However, in DP-models, it can only be considered in the *V-d* law. Regarding the ring beam effects, this can improve the behaviour of spandrels, which in turns leads to higher values of maximum peak strength of up to 25%. It can also be seen that the displacement, at which there is a more significant decay, due to the collapse of some of piers, is very similar to the one obtained in 3Muri.

5.4.2. Global behaviour

Two load patterns have been considered for the NLS analyses: uniform (solid lines) and pseudo-triangular (dotted lines). As can be observed in Fig. 21, the worst results in terms of peak strength and displacement capacity are obtained for the triangular load pattern in both directions. Note that for the sake of clarity, the axes scale is changed. It can be seen that the building presents a worse seismic capacity in the Y direction than in the X direction. This is due to the lack of resistant elements in the Y direction: there are only two lateral walls perpendicular to the main URM walls. As already mentioned at §5.4.1, the OpenSees LP-based models can reproduce better the behaviour of 3Muri while the DP models do not capture the initial cracked stiffness properly.

As analysed at the trilith scale, there is a variation of *N* acting in the panels during NLS analyses. In Fig. 22, this variation has been computed, for each of the modelling approaches, during the NLS in the X direction and for the piers located at the corners of the main wall. The *N* acting in piers, located at lower storeys and in the left part of the wall, decreases accordingly to the fact the analysis are performed in positive direction. It can be seen that *N* varies mainly in panels located at lower storeys while it varies slightly in the upper panels. In the case of 3Muri, the reduction of *N* in the pier located at the ground floor can be up to 47% while in OS, this reduction can be up to 58% and 43% for the DP-DF and LP-A models, respectively. Nevertheless, the increase of *N* in the pier located in the right part of the wall is 40%, 80% and 55% for the 3Muri, the DP-DF and LP-A models, respectively. The panels located at intermediate storeys, S2 and S3, can vary their *N* up to ±20%. The panels at upper storeys, S4 and S5, can vary their *N* by up to ±5%. Nevertheless, OpenSees models present lower percentages of variation for S2–S5 storeys than 3Muri and that variation doesn't affect the strength capacity of piers.

5.4.3. Damage

In this section, the expected seismic damage in each of the panels of the main and back URM walls is accounted for considering each failure mechanism: shear and flexural. The damage has been computed according to the strength of each panel previously analysed. It has been checked if each damage limit state (DLS) is activated by comparing the numerical results with the limits established in each constitutive law: *V-γ* or *V-d* for shear damage; and *M-θ*, for flexural damage. Each damage state corresponds to each of the limit values of the branches. In Fig. 23, the type of damage expected in each panel considering each modelling approach has been plotted. As can be observed, highly similar results are obtained in OpenSees compared to 3Muri in terms of type of damage. Most panels present a similar type of failure. The damage is concentrated in the same panels and areas of the walls. Furthermore, it can be noted that in all the

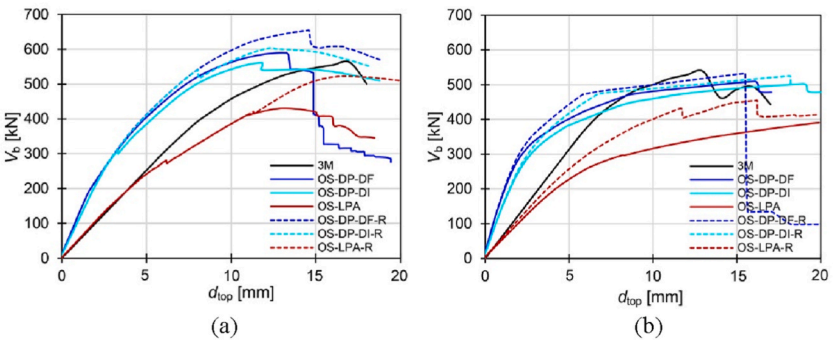

Fig. 20. Pushover curves of the (a) main and (b) back façades of the case study building.

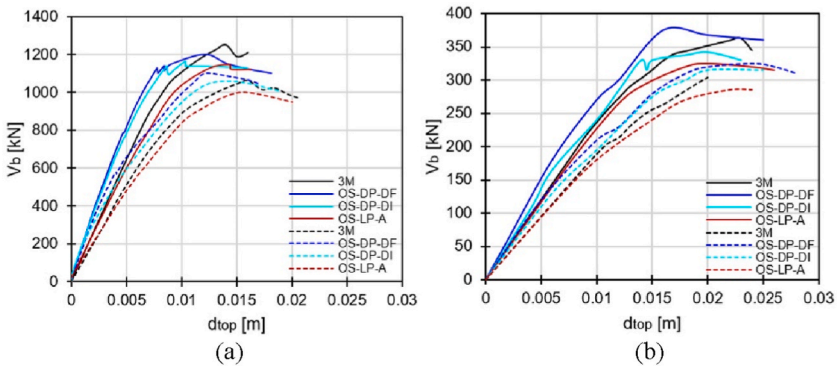

Fig. 21. Capacity curves of building in the (a) X and (b) Y direction considering the uniform (solid lines) and the triangular (dotted lines) load patterns.

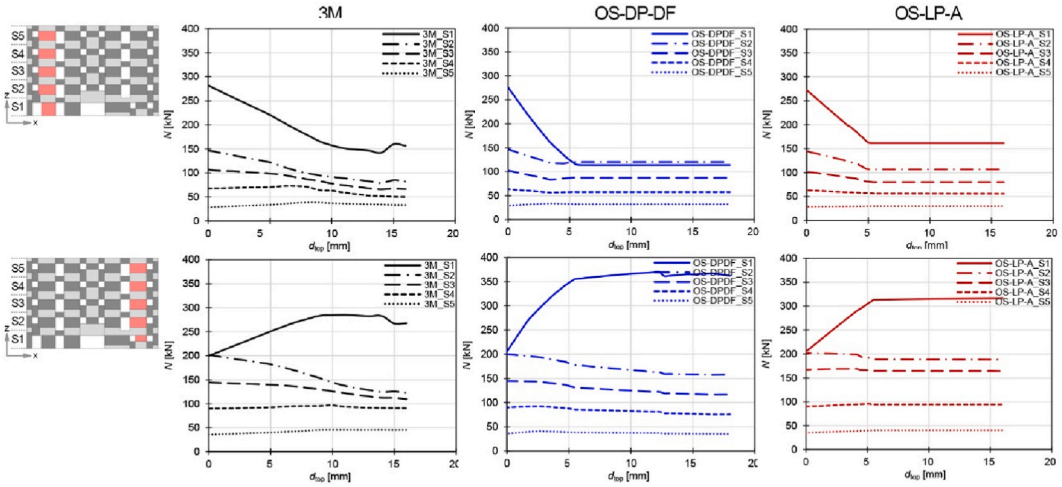

Fig. 22. Variation of *N* in piers at different storeys (S) according to the modelling approaches considered during the NLS in the X direction.

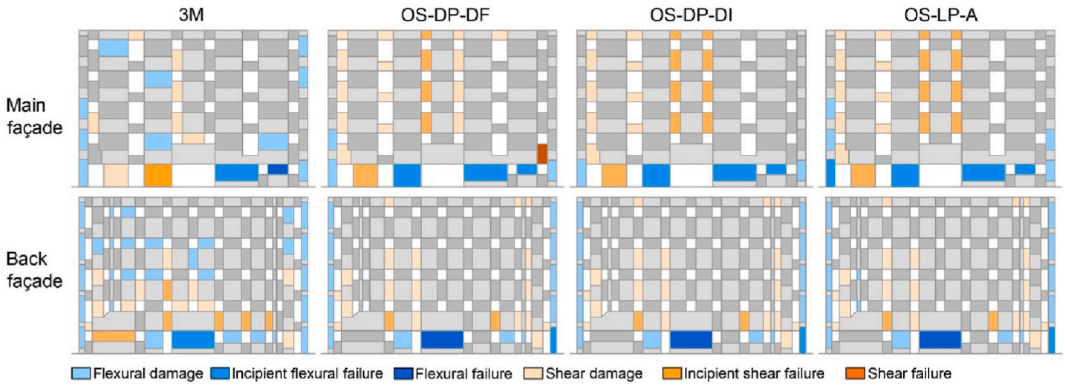

Fig. 23. EF mesh idealisation for each façade in each software package.

models, piers will mainly fail or be damaged due to flexural while spandrels due to shear. Regarding the main façade, damage is concentrated at the ground floor, leading to an incipient shear and flexural failure of some panels. Spandrels at the central part of the wall will present shear damage in all the models. Concerning, the back façade, this presents a larger number of panels that will be damaged. Again, damage will be concentrated at the ground floor, resulting in panels even failing.

6. Conclusions

This work has focused on comparing different EF modelling approaches for the seismic assessment of URM buildings. To do so, alternative elements in OpenSees have been tested considering different plasticity approaches. The response of some benchmark case studies, available in the literature from the '*URM nonlinear modelling* – Benchmark project' ReLUIS project, have been adopted to test the reliability of the alternative approaches considered. Moreover, the results have also been compared with the commercial software 3Muri, specifically conceived for performing nonlinear analyses on URM buildings.

At single panel and trilith scale, main conclusions achieved may be summarized as follows:

- Concerning the nonlinear constitutive law of DP-based models, values of 20% and 4% of f_{cm} to define the f_{cu} and the f_t, respectively, have resulted in the best simulations fitted of the target behaviour.
- At high ratios of σ/f_{cm}, the numerical results do not seem to properly fit the shear domain. This is related to the correct definition of the axial load acting in panels. Therefore, in structures with panels characterized by high ratios, if the properties of the shear hinges are not properly defined, the global results might not be reliable.
- No differences have been obtained if the axial load was applied either as a concentrated-nodal or a distributed load. However, in this work, concentrated loads were applied at the nodes as in 3Muri.
- LP-based models can better capture a similar cracked stiffness as to that in 3Muri. Contrariwise, DP-based models, owing to their difficulty to account for the degradation of the flexural behaviour, are not able to properly capture conventional assumptions on the cracked stiffness, like those also recommended in codes. Additionally, in the DP approach, the cracked stiffness can be considered by only modifying the properties of the shear hinge. Contrariwise, in the LP approach, the cracked stiffness can be borne in mind by decreasing both the initial stiffness of the shear hinge properties and the elastic material of the interior beam as in 3Muri. Hence, LP-based models can produce more similar results to 3Muri. These conclusions have been also obtained at the trilith and at the global building scale.

At a global building scale, main conclusions achieved may be summarized as follows:

- Concerning the values of the fundamental vibration periods and the modal shape vectors, similar modal results have been obtained for both the OpenSees and the 3Muri models.
- The systematic introduction of ring beams can lead to an increase of the maximum peak strength of up to 25% for this structure.
- The OpenSees curves highly match the reference results from 3Muri for the global building. However, there are some exceptions: LP-based models can reproduce the behaviour of 3Muri better; and the DP models do not capture the initial cracked stiffness properly, as concluded at the other scales.

As far the seismic vulnerability of the building examined concerns, it presents a worse seismic capacity in the Y direction than in the X direction. This is due to the lack of resistant elements in the Y direction: in fact, there are only two lateral walls perpendicular to the main URM walls. The main façade wall presents a higher seismic capacity than the back façade due to the distribution of openings. The back façade presents narrow piers and short spandrels, which leads to a higher concentration of damage at the early steps of the NLS analyses. Most panels present a similar type of failure and the damage is concentrated in the same panels and areas of the walls, mainly on the ground floor.

To sum up, the results have shown that the method proposed in this manuscript allows using OpenSees to accurately calculate masonry structures with nonlinear beam elements. This work represents a first step and several limitations have been identified during the research. Such is the case of the variation of the axial load acting in panels. As stated, in 3Muri this is automatically updated during the NLS analyses. However, in OpenSees this is not yet possible. According to the results of this study, this variation can be negligible at the upper storeys of the structures. Notwithstanding there is a considerable variation at ground floor panels. In this study, it has been noticed that this effect is only relevant on the ground floor (which is just one of the five plants of the case study building). Therefore, special careful should be taken into account if these modelling methods are applied to high URM buildings. Hence, further assessment of the implementation of the variation of the axial load in panels is suggested for future research work.

Additionally, in this work, it has been obtained that at lower ratios of σ/f_{cm}, panels show a tendency to be governed by a tensile behaviour. According to the numerical results obtained, it does not tend to be 0 and a certain tensile strength can be computed. Therefore, a specific analysis of the importance of the tensile strength should be performed in future analyses. This can be important in the modelling procedure of spandrels.

Finally, the outcomes of this paper may constitute, in future research, the basis for exploiting the potential and versatility of OpenSees in accounting for other tricky problem, which is the soil-foundation-structure interaction, that is worth to be investigated in Seville. The SSI effects have been investigated in previous studies in both software [15,65–67]. However, the preliminary analyses carried out in this paper will be very useful to start with models set on the basis of consistent assumptions and that are able to provide results already verified and in agreement under the fixed base hypothesis. The main goal is not the validation of the results with respect to the reality (already checked in other experiences), but the comparison between software under consistent hypotheses. In future works, the reliability of the numerical modes for existing buildings in Seville will be investigated, at least by considering free ambient vibration tests.

CRediT author statement

M.V. Requena-Garcia-Cruz: Conceptualization, Methodology, Investigation, Formal Analysis, Software, Validation, Writing -

Original Draft, Writing - Review & Editing, Funding acquisition, Project administration.

S. Cattari: Conceptualization, Methodology, Investigation, Data Curation, Validation, Writing - Review & Editing, Supervision.

R. Bento: Methodology, Validation, Writing - Review & Editing, Supervision.

A. Morales-Esteban: Conceptualization, Supervision, Writing - Review & Editing, Funding acquisition, Project administration.

Declaration of competing interest

The authors declare that they have no known competing financial interests or personal relationships that could have appeared to influence the work reported in this paper.

Data availability

Data will be made available on request.

Acknowledgements

This work has been supported by the **Spanish Ministry of Science and Innovation** through the **PID2020-117207RB-I00** project and the **Andalusian Government** through the **PROYEXCEL_00768** and the **US.20-01** projects. The first author would like to acknowledge the support provided by the **Spanish Ministry of Universities** through the **Margarita Salas fellowship** and the **VIII-PPI** of the **University of Seville**.

References

[1] A.M. D'Altri, V. Sarhosis, G. Milani, J. Rots, S. Cattari, S. Lagomarsino, E. Sacco, A. Tralli, G. Castellazzi, S. de Miranda, Modeling strategies for the computational analysis of unreinforced masonry structures: review and classification, Arch. Comput. Methods Eng. 27 (2020) 1153–1185, https://doi.org/10.1007/S11831-019-09351-X/FIGURES/20.

[2] S. Cattari, B. Calderoni, I. Caliò, G. Camata, S. de Miranda, G. Magenes, G. Milani, A. Saetta, Nonlinear modeling of the seismic response of masonry structures: critical review and open issues towards engineering practice, Bull. Earthq. Eng. 20 (2022) 1939–1997, https://doi.org/10.1007/S10518-021-01263-1.

[3] A.M. D'Altri, F. Cannizzaro, M. Petracca, D.A. Talledo, Nonlinear modelling of the seismic response of masonry structures: calibration strategies, Bull. Earthq. Eng. 20 (2022) 1999–2043, https://doi.org/10.1007/S10518-021-01104-1.

[4] S. Degli Abbati, P. Morandi, S. Cattari, E. Spacone, On the reliability of the equivalent frame models: the case study of the permanently monitored Pizzoli's town hall, Bull. Earthq. Eng. (2021) 1–31, https://doi.org/10.1007/S10518-021-01145-6/FIGURES/21.

[5] S. Lagomarsino, A. Penna, A. Galasco, S. Cattari, TREMURI program: an equivalent frame model for the nonlinear seismic analysis of masonry buildings, Eng. Struct. 56 (2013) 1787–1799, https://doi.org/10.1016/j.engstruct.2013.08.002.

[6] M. Dolce, Schematizzazione e modellazione degli edifici in muratura soggetti ad azioni sismiche (in Italian), L'industria Delle Costruzioni 25 (1991) 44–57.

[7] L. Sorrentino, S. Cattari, F. da Porto, G. Magenes, A. Penna, Seismic behaviour of ordinary masonry buildings during the 2016 central Italy earthquakes, Bull. Earthq. Eng. 17 (2019) 5583–5607, https://doi.org/10.1007/s10518-018-0370-4.

[8] N. Augenti, F. Parisi, Learning from construction failures due to the 2009 L'aquila, Italy, earthquake, J. Perform. Constr. Facil. 24 (2010) 536–555, https://doi.org/10.1061/(ASCE)CF.1943-5509.0000122.

[9] D.F. D'Ayala, S. Paganoni, Assessment and analysis of damage in L'Aquila historic city centre after 6th April 2009, Bull. Earthq. Eng. 9 (2011) 81–104, https://doi.org/10.1007/s10518-010-9224-4.

[10] M. Pavanetto, L. Sbrogiò, M. Salvalaggio, M.R. Valluzzi, Equivalent frame modelling of an unreinforced masonry building in finite element environment, Lecture Notes Mechan. Eng. 2 (2020) 2006–2021, https://doi.org/10.1007/978-3-030-41057-5_160.

[11] Italian Ministry of Infrastructures, Transportation (MIT), Istruzioni per l'applicazione dell'«Aggiornamento delle "Norme tecniche per le costruzioni"» di cui al decreto ministeriale 17 gennaio 2018 (Circular 21/1/19, No. 7 C.S.LL.PP), 2018 (in Italian), Rome, Italy.

[12] NZSEE, Assessment and Improvement of the Structural Performance of Buildings in Earthquake. Recommendations of a NZSEE Project Technical Group, 2006 (including Revision of Section 10 available online from: April 2015), Wellington, New Zealand.

[13] European Union, Eurocode-8: design of structures for earthquake resistance. Part 3: assessment and retrofitting of buildings, Brussels, Belgium, http://www.phd.eng.br/wp-content/uploads/2014/07/en.1998.3.2005.pdf, 2005.

[14] V. Cardinalli, M. Tanganelli, R. Bento, Seismic assessment of the XX century masonry buildings in Florence: vulnerability insights based on urban data acquisition and nonlinear static analysis, J. Build. Eng. (2022), https://doi.org/10.1016/j.jobe.2022.104801.

[15] A. Brunelli, F. de Silva, A. Piro, F. Parisi, S. Sica, F. Silvestri, S. Cattari, Numerical simulation of the seismic response and soil–structure interaction for a monitored masonry school building damaged by the 2016 Central Italy earthquake, Bull. Earthq. Eng. 19 (2021) 1181–1211, https://doi.org/10.1007/S10518-020-00980-3.

[16] M. Angiolilli, M. Eteme Minkada, M. di Domenico, S. Cattari, A. Belleri, G.M. Verderame, Comparing the observed and numerically simulated seismic damage: a unified procedure for unreinforced masonry and reinforced concrete buildings, J. Earthq. Eng. (2022) 1–37, https://doi.org/10.1080/13632469.2022.2096721.

[17] F. Vanin, A. Penna, K. Beyer, A three-dimensional macroelement for modelling the in-plane and out-of-plane response of masonry walls, Earthq. Eng. Struct. Dynam. 49 (2020) 1365–1387, https://doi.org/10.1002/EQE.3277.

[18] C. Morandini, D. Malomo, A. Penna, Equivalent frame discretisation for URM façades with irregular opening layouts, Bull. Earthq. Eng. (2022) 1–30, https://doi.org/10.1007/S10518-022-01315-0/TABLES/5.

[19] S. Cattari, A.M. D'Altri, D. Camilletti, S. Lagomarsino, Equivalent frame idealization of walls with irregular openings in masonry buildings, Eng. Struct. 256 (2022), https://doi.org/10.1016/J.ENGSTRUCT.2022.114055.

[20] S. Cattari, D. Camilletti, A.M. D'Altri, S. Lagomarsino, On the use of continuum Finite Element and Equivalent Frame models for the seismic assessment of masonry walls, J. Build. Eng. 43 (2021), 102519, https://doi.org/10.1016/j.jobe.2021.102519.

[21] D. Ottonelli, C.F. Manzini, C. Marano, E.A. Cordasco, S. Cattari, A comparative study on a complex URM building: part I—sensitivity of the seismic response to different modelling options in the equivalent frame models, Bull. Earthq. Eng. 20 (2022) 2115–2158, https://doi.org/10.1007/s10518-021-01128-7.

[22] C.F. Manzini, D. Ottonelli, S.D. Abbati, C. Marano, E.A. Cordasco, Modelling the seismic response of a 2-storey URM benchmark case study: comparison among different equivalent frame models, Bulletin Earthquake Eng. SI: URM no (2020), https://doi.org/10.1007/s10518-021-01173-2.

[23] C. Calderini, S. Cattari, S. Lagomarsino, In-plane strength of unreinforced masonry piers, Earthq. Eng. Struct. Dynam. 38 (2009) 243–267, https://doi.org/10.1002/eqe.860.

[24] K.M. Dolatshahi, M.T. Nikoukalam, K. Beyer, Numerical study on factors that influence the in-plane drift capacity of unreinforced masonry walls, Earthq. Eng. Struct. Dynam. 47 (2018) 1440–1459, https://doi.org/10.1002/eqe.3024.

[25] S. Cattari, G. Magenes, Benchmarking the software packages to model and assess the seismic response of unreinforced masonry existing buildings through nonlinear static analyses, Bull. Earthq. Eng. 20 (2022) 1901–1936, https://doi.org/10.1007/S10518-021-01078-0.

[26] J. Milosevic, S. Cattari, R. Bento, Definition of fragility curves through nonlinear static analyses: procedure and application to a mixed masonry-RC building stock, Bull. Earthq. Eng. 18 (2020) 513–545, https://doi.org/10.1007/S10518-019-00694-1/FIGURES/18.
[27] G. Magenes, Masonry building design in seismic areas: recent experiences and prospects from a European standpoint, in: 1st European Conference on Earthquake Engineering and Seismology, 2006, pp. 3–8.
[28] E. Spacone, F.C. Filippou, F.F. Taucer, Fibre beam-column model for non-linear analysis of R/C frames : Part I. Formulation, Earthq. Eng. Struct. Dynam. 25 (1996) 711–725, https://doi.org/10.1002/(SICI)1096-9845 (199607)25:7<711::AID-EQE576>3.0.CO;2-9.
[29] CDS Win – STS Web, (n.d.). https://www.stsweb.it/cds-win/(accessed December 7, 2022).
[30] J.P. Conte, M. Barabato, E. Spacone, Finite element response sensitivity analysis using force-based frame models, Int. J. Numer. Methods Eng. 59 (2004) 1781–1820, https://doi.org/10.1002/NME.994.
[31] Y. Belmouden, P. Lestuzzi, An equivalent frame model for seismic analysis of masonry and reinforced concrete buildings, Construct. Build. Mater. 23 (2009) 40–53, https://doi.org/10.1016/J.CONBUILDMAT.2007.10.023.
[32] R. Siano, P. Roca, G. Camata, L. Pelà, V. Sepe, E. Spacone, M. Petracca, Numerical investigation of non-linear equivalent-frame models for regular masonry walls, Eng. Struct. 173 (2018) 512–529, https://doi.org/10.1016/j.engstruct.2018.07.006.
[33] S. Capdevielle, S. Grange, F. Dufour, C. Desprez, A shear warping kinematic enhancement for fiber beam elements with a damaging cross-section, Finite Elem. Anal. Des. 195 (2021), 103559, https://doi.org/10.1016/j.finel.2021.103559.
[34] J.M. Bairan Garcia, A.R. Mari Bernat, Shear-bending-torsion interaction in structural concrete members: a nonlinear coupled sectional approach, Arch. Comput. Methods Eng. 14 (2007) 249–278, https://doi.org/10.1007/s11831-007-9007-5.
[35] F. McKenna, G.L. Fenves, M.H. Scott, OpenSees: open system for earthquake engineering simulation, Pacific Earthquake Engineering, Research Center, University of California, Berkeley, 2000. http://opensees.berkeley.edu.
[36] E. Raka, E. Spacone, V. Sepe, G. Camata, Advanced frame element for seismic analysis of masonry structures: model formulation and validation, Earthq. Eng. Struct. Dynam. 44 (2015) 2489–2506, https://doi.org/10.1002/eqe.2594.
[37] M. Peruch, E. Spacone, G. Camata, Nonlinear analysis of masonry structures using fiber-section line elements, Earthq. Eng. Struct. Dynam. 48 (2019) 1345–1364, https://doi.org/10.1002/eqe.3188.
[38] G. Camata, C. Marano, V. Sepe, E. Spacone, R. Siano, M. Petracca, P. Roca, L. Pelà, Validation of non-linear equivalent-frame models for irregular masonry walls, Eng. Struct. 253 (2022), 113755, https://doi.org/10.1016/j.engstruct.2021.113755.
[39] A. Shabani, M. Kioumarsi, A novel macroelement for seismic analysis of unreinforced masonry buildings based on MVLEM in OpenSees, J. Build. Eng. 49 (2022), https://doi.org/10.1016/J.JOBE.2022.104019.
[40] S. Cattari, K. Beyer, Influence of spandrel modelling on the seismic assessment of existing masonry buildings, in: Proceedings of the Tenth Pacific Conference on Earthquake Engineering Building an Earthquake-Resilient Pacific, 2015, pp. 88–95.
[41] S. Lagomarsino, S. Cattari, D. Ottonelli, The heuristic vulnerability model: fragility curves for masonry buildings, Bull. Earthq. Eng. 19 (2021) 3129–3163, https://doi.org/10.1007/S10518-021-01063-7/TABLES/19.
[42] K. Beyer, S. Mangalathu, Review of strength models for masonry spandrels, Bulletin Earthquake Eng. 11 (2013) 521–542, https://doi.org/10.1007/s10518-012-9394-3.
[43] V. Sepe, E. Spacone, E. Raka, G. Camata, Seismic analysis of masonry buildings: equivalent frame approach with fiber beam elements, in: 9th International Conference on Structural Dynamics, EURODYN, 2014, pp. 237–244.
[44] S. Bracchi, A. Galasco, A. Penna, A novel macroelement model for the nonlinear analysis of masonry buildings. Part 1: axial and flexural behavior, Earthq. Eng. Struct. Dynam. 50 (2021) 2233–2252, https://doi.org/10.1002/EQE.3445.
[45] S. Popovics, A numerical approach to the complete stress-strain curve of concrete, Cement Concr. Res. 3 (1973).
[46] M. Petracca, F. Candeloro, G. Camata, STKO User Manual", ASDEA Software Technology, Pescara, Italy, 2017.
[47] A. Penna, S. Lagomarsino, A. Galasco, A nonlinear macroelement model for the seismic analysis of masonry buildings, Earthq. Eng. Struct. Dynam. 43 (2014) 159–179, https://doi.org/10.1002/eqe.2335.
[48] Ministero delle infrastrutture e dei trasporti, NTC, Aggiornamento delle «Norme tecniche per le costruzioni», 2018. Italy.
[49] A. Belarbi, T.T.C. Hsu, Constitutive laws of concrete in tension and reinforcing bars stiffened by concrete, Structural J. 91 (1994) 465–474, https://doi.org/10.14359/4154.
[50] S. Cattari, D. Camilletti, S. Lagomarsino, S. Bracchi, M. Rota, A. Penna, Masonry Italian code-conforming buildings. Part 2: nonlinear modelling and time-history analysis, J. Earthq. Eng. 22 (2018) 2010–2040, https://doi.org/10.1080/13632469.2018.1541030.
[51] K. Beyer, M. Eeri, A. Dazio, Quasi-static cyclic tests on masonry spandrels. https://doi.org/10.1193/1.4000063, 2012.
[52] V. Turnšek, F. Čačovič, Some experimental results on the strength of brick masonry walls, in: Proc. Of the Second International Brick Masonry Conference, Stoke-on-Trent, England, 1971, pp. 149–156.
[53] G. Magenes, G.M. Calvi, In-plane seismic response of brick masonry walls, Earthq. Eng. Struct. Dynam. 26 (1996) 1091–1112, https://doi.org/10.1002/(SICI)1096-9845 (199711)26:11.
[54] D. Abrams, N. Shah, Cyclic Load Testing of Unreinforced Masonry Walls, 1992. Illinois.
[55] L.M. Massone, J.W. Wallace, Analytical Modeling of Reinforced Concrete Walls for Predicting Flexural and Coupled-Shear-Flexural Responses Kutay Orakcal, 2006.
[56] A. Anthoine, G. Magonette, Shear-compression testing and analysis of brick masonry walls, in: 10th European Conference on Earthquake Engineering, 1994. Viena.
[57] M. Corradi, A. Borri, A. Vignoli, Experimental study on the determination of strength of masonry walls, Construct. Build. Mater. 17 (2003) 325–337, https://doi.org/10.1016/S0950-0618(03)00007-2.
[58] F. Pérez-Gálvez, C. Rodríguez-Liñán, P. Rubio, Determination of the mechanical characteristics of masonry walls of the traditional housing in Sevilla between 1700 and 1900, Inf. Construcción 61 (2009) 19–28, https://doi.org/10.3989/IC.06.001.
[59] A. Vignoli, S. Boschi, N. Signorini, Abaco Delle Murature Della Regione Toscana, Protocolli di prova, Florence, 2019.
[60] M. Angiolilli, S. Lagomarsino, S. Cattari, S. Degli Abbati, Seismic fragility assessment of existing masonry buildings in aggregate, Eng. Struct. 247 (2021), 113218, https://doi.org/10.1016/J.ENGSTRUCT.2021.113218.
[61] European Union, Eurocode-6: Design of Masonry Structures. Part 1-1: General Rules for Reinforced and Unreinforced Masonry Structures, 2005. Brussels.
[62] Spanish Ministry of Housing, MV-201.Unreinforced ceramic masonry walls [Muros resistentes de fábrica de ladrillo], 1972.
[63] M.V. Requena-Garcia-Cruz, A. Morales-Esteban, P. Durand-Neyra, Optimal ductility enhancement of RC framed buildings considering different non-invasive retrofitting techniques, Eng. Struct. 242 (2021), 112572, https://doi.org/10.1016/j.engstruct.2021.112572.
[64] M. Pastor, M. Binda, T. Harčarik, Modal assurance criterion, in: Procedia Eng, Elsevier Ltd, 2012, pp. 543–548, https://doi.org/10.1016/j.proeng.2012.09.551.
[65] M.V. Requena-Garcia-Cruz, A. Morales-Esteban, P. Durand-Neyra, Assessment of specific structural and ground-improvement seismic retrofitting techniques for a case study RC building by means of a multi-criteria evaluation, Structures 38 (2022) 265–278, https://doi.org/10.1016/j.istruc.2022.02.015.
[66] M.V. Requena-Garcia-Cruz, R. Bento, P. Durand-Neyra, A. Morales-Esteban, Analysis of the soil structure-interaction effects on the seismic vulnerability of mid-rise RC buildings in Lisbon, Structures 38 (2022) 599–617, https://doi.org/10.1016/j.istruc.2022.02.024.
[67] M.V. Requena-Garcia-Cruz, E. Romero-Sánchez, A. Morales-Esteban, Numerical investigation of the contribution of the soil-structure interaction effects to the seismic performance and the losses of RC buildings, Develop. Built Environ. 12 (2022), 100096, https://doi.org/10.1016/j.dibe.2022.100096.